



# Experimental Investigation on Shear Mechanical Behavior of Sandstone Containing a Pre-existing Flaw Under Unloading Normal Stress with Constant Shear Stress

Da Huang<sup>1,2</sup> · Ying-Quan Guo<sup>1</sup> · Duo-Feng Cen<sup>1</sup> · Zhu Zhong<sup>1</sup> · Yi-Xiang Song<sup>1</sup>

Received: 15 December 2019 / Accepted: 16 April 2020 / Published online: 7 May 2020  
© Springer-Verlag GmbH Austria, part of Springer Nature 2020

## Abstract

Excavation, river incision and anchor cable relaxation would result in unloading of stress in at least one direction of rock masses in caverns or slopes, and the unloading failure is prominent and it even shows remarkable tensile failure. The previous direct shear tests with constant normal stress can no longer meet these circumstances. However, the experimental study of rock shear behavior under unloading normal stress condition is rare. This paper presents an innovative experimental method to study the mechanical behaviors of sandstone containing a pre-existing flaw under unloading normal stress with constant shear stress. Five failure patterns were identified based on the analysis of crack propagation and their mechanical properties. The failure pattern transforms from mixed tensile–shear failure to tensile failure then to shear failure with the increase of flaw angle. Initial normal stress is greater, the propagating cracks behave as stronger tensile fractures. The peak dilatancy angle increases and decreases with the increase of the initial normal and shear stresses, respectively. Internal friction angle and cohesion both decrease first and then increase with the increase of flaw angle. The branch crack, extent of exfoliation, shear scratch and failure pattern are different from that in the traditional direct shear tests. Unloading normal stress significantly weakens the shear strength compared to traditional direct shear tests, suggesting that the shear strength parameters used in stability evaluation of rock excavation engineering should be determined by unloading tests. The results enrich the basic theory of rock mechanics.

**Keywords** Fissured rock mass · Shear behavior · Failure pattern · Unloading normal stress · Flaw angle

## 1 Introduction

The mechanical essence of excavation (e.g., mining, excavated slopes and underground caverns), river incision and anchor cable relaxation are causing stress redistribution in rock masses and unloading of stress in one or more directions additionally (Cho et al. 2008; Huang and Huang 2014; Cen and Huang 2017; Cen et al. 2020; Huang et al. 2020). In the processes of these conditions mentioned above, the

stresses in rock masses decrease in the direction perpendicular to the free face and possibly increase in the direction parallel to the free face before failure of rock masses, which makes the disturbed rocks more prone to shear failure (because of the decrease of the normal stress) or tensile splitting failure (due to the decrease of the lateral pressure) (Fig. 1). In addition, there are a lot of multi-scale internal defects in rock masses, which affect the fracturing responses and mechanical properties such as deformation and strength significantly (Gehle and Kutter 2003; Cai and Kaiser 2005; Zhou et al. 2014; Yin et al. 2017, 2018, 2019). Therefore, knowledge of shear mechanical behavior of flawed rock masses under unloading normal stress is important to interpret and predict geo-hazards concerning rock landslides and collapses as well as surrounding rock failure of underground engineering.

The shear mechanical behaviors of flawed rock mass with constant normal stress has been experimentally investigated extensively, and the research emphasis is the effect

✉ Ying-Quan Guo  
201811601014@stu.hebut.edu.cn

✉ Duo-Feng Cen  
duofengcen@hebut.edu.cn

<sup>1</sup> School of Civil and Transportation Engineering, Hebei University of Technology, Tianjin 300401, China

<sup>2</sup> College of Geology Engineering and Geomatics, Chang'an University, Xi'an 710054, China

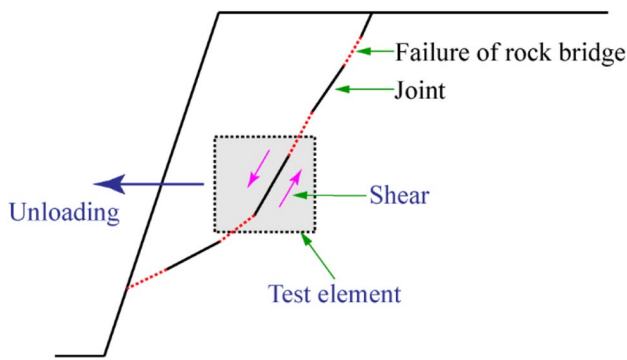


**Fig. 1** Schematic diagram of unloading failure of a rock slope with intermittent joints

of flaw geometrical and mechanical properties on the shear mechanical behaviors (Wong et al. 2004a; Wong and Einstein 2009). The flaw geometric parameters mainly include inclination angle, length number of flaw sets and the rock bridge parameters (namely bridge angle and length) (Wong et al. 2001, 2004b). Mechanical behaviors of rock specimens containing a single flaw are affected a lot by flaw angles.

About unloading, lots of experiments have been carried out to investigate its mechanical behaviors, in which they obtained remarkable achievements. Stress path, as one of the most important influencing factors, has been studied extensively (Huang and Li 2014; Huang and Zhu 2018, 2019; Huang et al. 2019; Zeng et al. 2019). Zhu and Huang (2019) investigated the shear mechanical behavior of intact rock specimens under unloading normal stress. The results indicated that the shear mechanical behaviors in the direct shear test under unloading normal stress were obviously different from that in the traditional direct shear test. The tests of rock specimens containing a parallel fissure pair under unloading normal stress with constant shear stress were carried out by Zhong et al. (2020). It was revealed that the impacts of the rupture surfaces of the unloading tests were narrower than those of the tradition direct shear tests.

As just mentioned, although experimental studies of intact rock and specimens containing a parallel fissure pair have been performed for the direct shear tests under unloading normal stress with constant shear stress, single-flawed specimens have not yet been carried out comprehensively nor well compared with the traditional direct shear test. Thus, it is necessary to systematically study the shear mechanical behaviors of rock specimens containing a single flaw under unloading normal stress with constant shear stress, especially for deformation characteristics, strength characteristic and crack evolution. In this paper, the influences of different flaw angles and initial stress levels on shear mechanical behaviors were analyzed, and the comparison with the direct shear tests with constant normal stress was discussed.

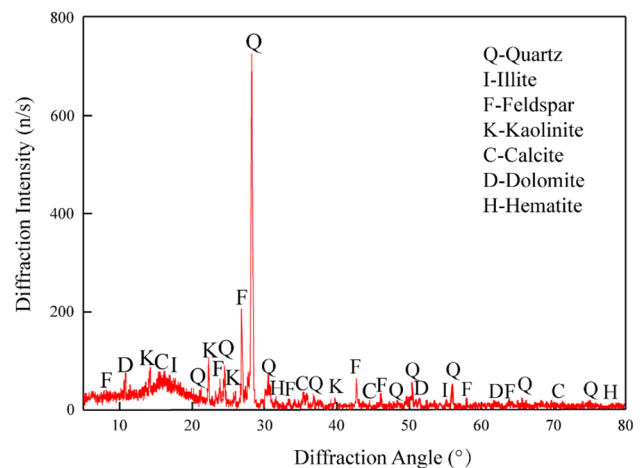


**Fig. 2** XRD spectrum of tested red sandstone

## 2 Experimental Program

### 2.1 Specimen Preparation

The tested rock is red sandstone from Chongqing, China. For the sake of reducing the influence of material dispersion on the tests, all specimens were cut from an intact rock block. The component of rock specimens, including quartz, illite, feldspar, kaolinite and a small quantity of calcite, dolomite, and hematite, were determined via X-ray diffraction (XRD) analysis (Zhu and Huang 2019), as shown in Fig. 2. Table 1 shows main mechanical properties of the red sandstone.

The overall dimension of specimens containing a pre-existing flaw is 60 mm wide  $\times$  60 mm long  $\times$  40 mm thick, as shown in Fig. 3a. As in extensive earlier experimental and theoretical work about fracturing behavior in flawed rocks or similar materials under different stress states, the term “flaw” was used to describe the artificially created fracture and the term “crack” was used to describe the newly propagating fracture (Wong and Einstein 2009; Zhou et al. 2014). In this paper, the naming rule will be followed. The flaws were created using a high-pressure water jet, the midpoint of flaws coincided with the geometric center of specimens. The length and aperture of all pre-existing flaws are 15 mm and 1 mm, respectively, as shown in Fig. 3a.

The geometry of a flaw is defined by flaw angle  $\beta$  (the angle that a flaw rotates to horizontal direction clockwise).  $\beta$  varies between  $0^\circ$  and  $160^\circ$  in  $20^\circ$  intervals (except  $\beta = 90^\circ$ ), namely there are eight different flaw angles ( $0^\circ$ ,  $20^\circ$ ,  $40^\circ$ ,  $60^\circ$ ,  $90^\circ$ ,  $120^\circ$ ,  $140^\circ$ ,  $160^\circ$ ), as shown in Fig. 3b.

### 2.2 Test Equipment and Procedure

In this paper, the direct shear test under unloading normal stress with constant shear stress (DSTUNS), as well as the

**Table 1** Main mechanical properties of tested red sandstone

Density $\rho$ (g/cm <sup>3</sup> )	Young's modulus $E$ (GPa)	UCS $\sigma_c$ (MPa)	Uniaxial tensile strength $\sigma_t$ (MPa)	Poisson's ratio $\nu$	Cohesion $c$ (MPa)	Internal friction angle $\varphi$ (°)
2.39	3.30	52	3.01	0.193	11.22	35.9

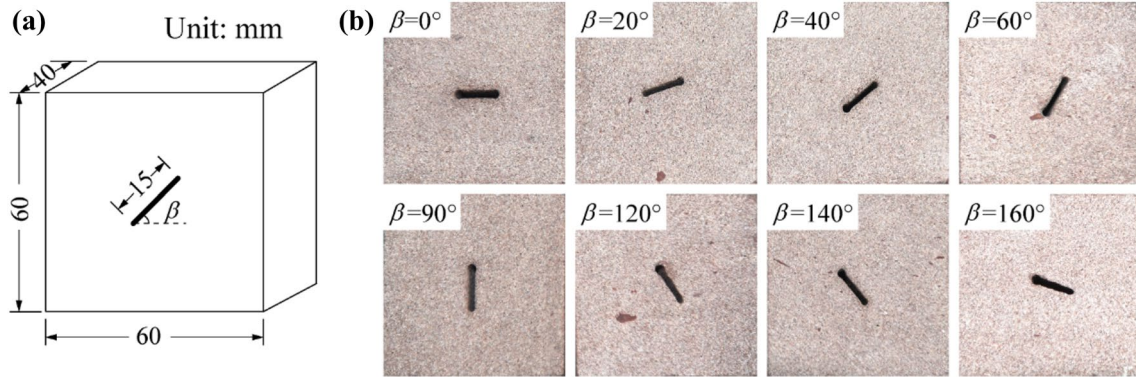


**Fig. 3** Geometry of the rock specimens. **a** Geometry; **b** specimens with variable flaw angles

direct shear test with constant normal stress (DSTCNS), were conducted by an electro-hydraulic servo rock shear testing machine which had a loading capacity of 600 kN in both vertical and horizontal directions. A simple auxiliary device containing upper and lower shear boxes and corresponding two rows of anti-friction plate embedded with steel balls were designed for this test, as shown in Fig. 4a. The auxiliary device could ensure the normal stress and shear stress be transferred to the shear surface. Under the action of the vertical force (normal force),  $F_v$ , and horizontal force (shear force),  $F_h$ , the middle surface of the rock specimen was subjected to a normal stress ( $\sigma$ ) and shear stress ( $\tau$ ). In addition, the displacements (vertical displacement and shear displacement) and the evolution processes of cracks were captured by four displacement gauges and the high speed video camera, respectively.

In the DSTUNS, force-controlled mode was adopted during the process of loading and unloading, the loading and unloading rate was 0.05 kN/s. In the DSTCNS, displacement-controlled mode was adopted during the process of loading shear stress, the loading rate was 0.2 mm/min. The mode and rate of loading normal stress process was the same with the DSTUNS. The DSTUNS procedure consists of three steps, as illustrated in Fig. 4b.

*1st step* loading the normal stress to the initial/target normal stress (INS)  $\sigma_{ni}$  (section AB in Fig. 4b). The INS  $\sigma_{ni}$  should be less than uniaxial compression strength  $\sigma_c$  to ensure the specimen not fail in the process of loading normal stress. According to uniaxial compression tests, the minimum value of uniaxial compressive strength is 41 MPa when the flaw angle is 60°. Therefore, five stress

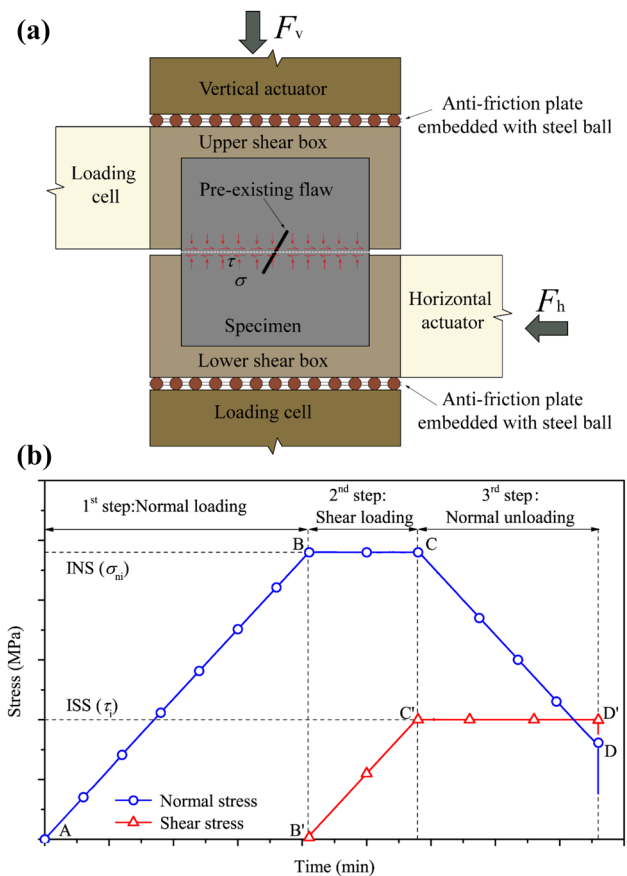


**Fig. 4** Schematics of the direct shear test under unloading normal stress. **a** Layout of the test system; **b** schematic of stress path

levels with equal intervals, i.e., 8 MPa, 16 MPa, 24 MPa, 32 MPa and 40 MPa, were chosen as initial normal stresses.

*2nd step* loading the shear stress to the initial/target shear stress (ISS)  $\tau_i$  (section B'C' in Fig. 4b) with the constant normal stress (section BC in Fig. 4b). The ISS  $\tau_i$  should be greater than the pure shear strength (i.e., the shear strength when the normal stress is 0) to ensure the specimen fail in the process of unloading normal stress (3rd step) but should not be greater than the shear strength under the constant normal stress of 8 MPa to prevent the specimen from failure in loading shear stress for the cases of minimal  $\sigma_{ni}$ . According to the direct shear tests in different flaw angles, the minimum value of shear strength is 6 MPa when the constant normal stress is 1 MPa (pure shear test is difficult to carry out; therefore, 1 MPa normal stress was applied) and the maximum value of shear strength is 15 MPa when the constant normal stress is 8 MPa. Therefore, five stress levels with equal intervals, i.e., 6 MPa, 8 MPa, 10 MPa, 12 MPa and 14 MPa were chosen as initial shear stresses.

*3rd step* unloading the normal stress (section CD in Fig. 4b) with the constant ISS  $\tau_i$  (section C'D' in Fig. 4b) until the specimen fails.

In this study, three possible influencing factors were considered, namely, the flaw angle ( $\beta$ ), initial normal stress level (INS  $\sigma_{ni}$ ), and initial shear stress level (ISS  $\tau_i$ ). In order to compare with the DSTUNS, a group of DSTCNS was carried out. Totally, 120 specimens are classified as three groups to investigate different conditions, as illustrated in Tables 2 and 3. The test of each sample number will be repeated using two specimens. Three groups of tests are as follows in detail:

**Group A:** In this group, the influence of two factors, which are flaw angle ( $\beta$ ) and initial normal stress (INS  $\sigma_{ni}$ ), are studied. The initial shear stress (ISS  $\tau_i$ ) is fixed at 10 MPa, and different initial normal stresses ( $\sigma_{ni}$ =8 MPa, 16 MPa, 24 MPa, 32 MPa and 40 MPa) and flaw angles ( $\beta$ =0°, 20°, 40°, 60°, 90°, 120°, 140° and 160°) are applied.

**Group B:** In this group, the influence of two factors, which are flaw angle ( $\beta$ ) and initial shear stress (ISS  $\tau_i$ ) are studied. The initial normal stress (INS  $\sigma_{ni}$ ) is fixed at 24 MPa, and different initial shear stresses ( $\tau_i$ =6 MPa, 8 MPa, 10 MPa, 12 MPa and 14 MPa) and flaw angles ( $\beta$ =0°, 20°, 40°, 60°, 90°, 120°, 140° and 160°) are applied.

**Group C:** A group of the traditional direct shear test was carried out. In order to study the influence of initial stress on the two kinds of tests, the normal stress of a series is

**Table 2** Geometry and load conditions of the rock specimens in the unloading normal stress test with constant shear stress

Test group	Sample number	Flaw angle $\beta$ (°)	INS $\sigma_{ni}$ (MPa)	ISS $\tau_i$ (MPa)
Group A	N0-1-N160-1	0-160	8	10
	N0-2-N160-2	0-160	16	10
	N0-3-N160-3	0-160	24	10
	N0-4-N160-4	0-160	32	10
	N0-5-N160-5	0-160	40	10
Group B	S0-1-S160-1	0-160	24	6
	S0-2-S160-2	0-160	24	8
	S0-3-S160-3	0-160	24	10
	S0-4-S160-4	0-160	24	12
	S0-5-S160-5	0-160	24	14

**Table 3** Geometry and normal stress of the rock specimens in the direct shear tests

Test group	Sample number	Flaw angle $\beta$ (°)	Normal stress $\sigma_n$ (MPa)					
Group C	C0-1-C160-1	0-160	24					
	C0-7-C160-7	0-160	1					
	C0-8-C160-8	0-160	8					
	C0-2-C0-6	0	0.53	2.48	4.44	6.40	8.36	
	C20-2-C20-6	20	2.50	4.63	6.73	9.40	12.50	
	C40-2-C40-6	40	2.86	5.50	8.90	12.00	16.12	
	C60-2-C60-6	60	4.49	6.70	10.00	12.52	15.63	
	C90-2-C90-6	90	3.97	6.13	8.78	11.00	13.13	
	C120-2-C120-6	120	3.11	5.33	7.55	9.77	11.99	
	C140-2-C140-6	140	2.51	4.58	7.02	8.90	10.79	
	C160-2-C160-6	160	1.92	3.55	5.29	7.50	9.84	

24 MPa, which is the same with the group B. In addition, in order to study the influence of stress state when failure happens, the normal stress of a series is set as the failure normal stress (namely the normal stress when the unloading failure happens) in the DSTUNS.

### 3 Test Results and Analysis

#### 3.1 Failure

##### 3.1.1 Failure Pattern

Whole failure processes of all specimens were recorded by the high speed video camera. By studying these videos and pictures taken in the DSTUNS, all failure patterns are summarized in Fig. 5. In Fig. 5, “T” represents tensile crack and “S” represents shear crack. The characteristic of tensile crack appears as the degree of grain opening, while the characteristic of shear crack appears as the shear displacement between grains and the exfoliation of the rock surface. In addition, the characteristic of fracture surface has distinct differences: the section of tensile crack is rough obviously and does not have striation, while the section of shear crack is smooth and has white striated scratch. Based on the evolution and the type of cracks, it is easy to identify the failure patterns as follow:

1. *Shear failure pattern* Shear crack initiates from the pre-existing flaw tip, at the same time, the shear crack extends from the specimen boundary to the pre-existing flaw tip. Then shear cracks and pre-existing flaw coalesce and the specimen fails (as shown in Fig. 5a). This pattern happens when  $\beta=0^\circ, 20^\circ, 140^\circ, 160^\circ$ .
2. *Tensile failure pattern* In the unloading process, the cracks are all tensile cracks, which initiate from pre-existing flaw tip and extend to the specimen boundary, finally coalesce. The Angle between the tensile failure plane and the shear direction is small (as shown in Fig. 5b). This pattern happens when  $\beta=40^\circ-90^\circ$ .
3. *Tensile–shear mixed failure pattern* There are both shear crack and tensile crack in the propagation cracks. The propagation and evolution of tensile cracks and shear cracks are different, as well as the distribution areas. Thus, tensile–shear mixed failure pattern can be divided into three subclasses as follows:

- (a) In this pattern, tensile crack initiates from the tip of the pre-existing flaw. When the tensile crack extends to a certain point in the middle of the specimen, it changes to shear crack and extends to the edge of the specimen sequentially in the direction parallel to the shear direction, as shown in Fig. 5c. This pattern happens when  $\beta=0^\circ-160^\circ$ .

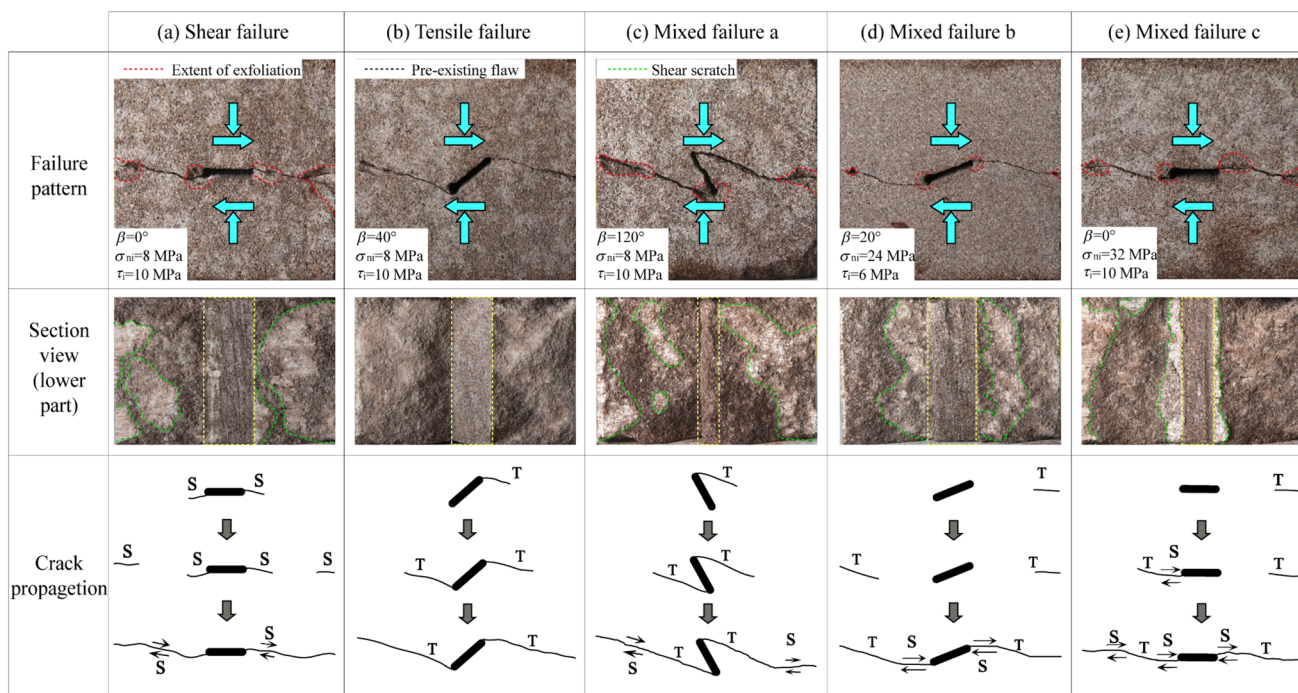


Fig. 5 Typical failure patterns of specimens containing a pre-existing flaw in the DSTUNS

- (b) In this pattern, tensile crack initiates from the boundary of the specimen (usually starts from the side that shear stress applied), then it propagates to the middle of the specimen, finally tensile crack changes to shear crack and coalesced with the tip of the pre-existing flaw (the direction of the shear crack is also nearly parallel to the shear direction), as shown in Fig. 5d. This pattern happens when  $\beta = 0^\circ\text{--}40^\circ$ .
- (c) In this pattern, crack appears as three sections that “shear–tensile–shear”. Tensile crack initiates from the boundary of the specimen that shear stress applied, and extends horizontally, then changes to shear crack coalescing with the tip of the pre-existing flaw. Meanwhile, shear crack extends from the boundary of the specimen that far away from the shear stress applied, then changes to tensile crack, finally coalesces, as shown in Fig. 5e. This pattern happens when  $\beta = 0^\circ, 90^\circ, 120^\circ, 140^\circ$ . It should be noted that, the influencing factor of failure pattern is not only the flaw angle but also initial normal stress and initial shear stress. Therefore, specimens with the same flaw may have different failure patterns, because they are under the different initial normal stress or initial shear stress. For instant, in the condition of  $\beta = 0^\circ$ , when initial normal stress is 24 MPa and initial shear stress is 10 MPa, the failure pattern is (a),

while initial normal stress is 32 MPa and initial shear stress is 10 MPa, the failure pattern is (c).

The ultimate failure patterns of sandstone specimens of all geometry and stress conditions are summarized in Fig. 6. The effects of flaw angles and initial normal and shear stress on the failure patterns have obvious regularity, which will be discussed in the following sections, respectively.

### 3.1.2 Influence of Flaw Angle

The influences of flaw angles on failure patterns have been shown in Fig. 7. The area of exfoliation is smaller and smaller with the increase of flaw angles. Once the flaw angle is greater than  $60^\circ$ , the area of exfoliation is larger and larger with the increase of flaw angles. Exfoliation occurs mainly near the boundary of specimens, far from the pre-existing flaw tip. The area of shear scratch has the same variation trend. As to the failure pattern, the variation trend is from mixed tensile–shear failure to tensile failure with the flaw angle increasing to  $60^\circ$  (Fig. 7d). When the flaw angle continues increasing, the failure pattern becomes mixed tensile–shear failure. Finally, shear failure occurs when the flaw angle becomes  $160^\circ$ .

**Fig. 6** Evolution law of failure patterns of sandstone specimens

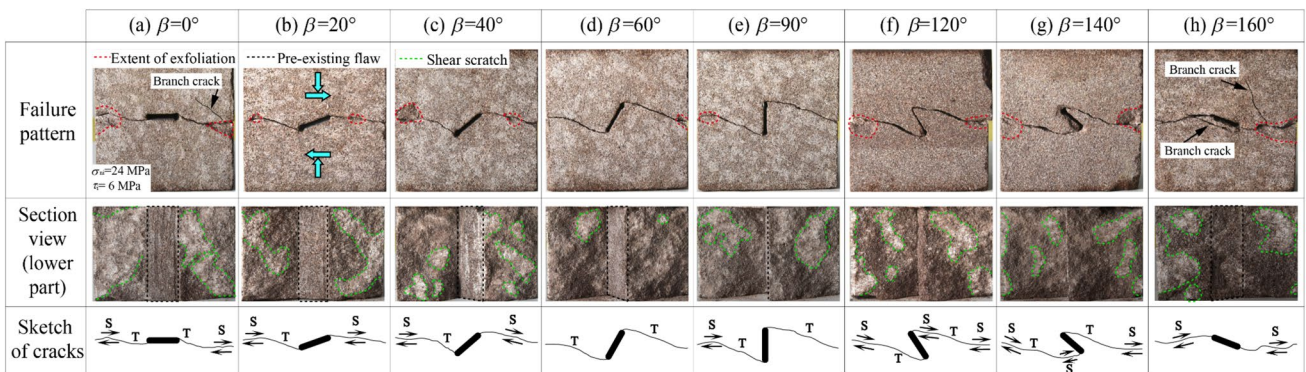
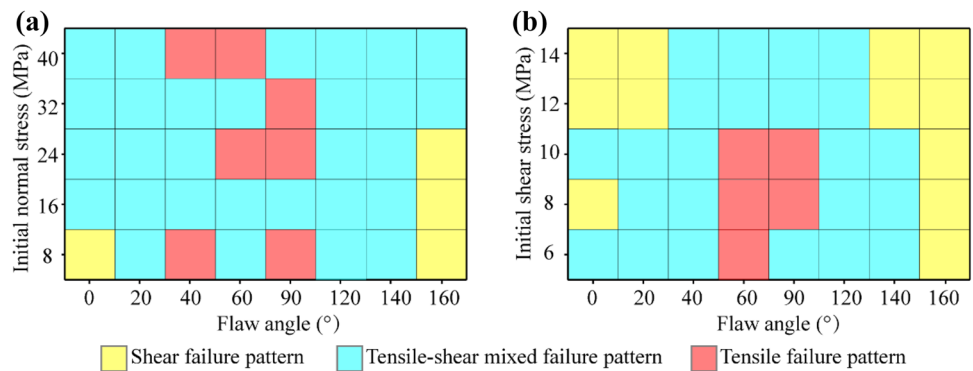


**Fig. 7** Failure patterns of specimens with different flaw angles

As shown in Fig. 8, the relationship between deformation and failure pattern is close and regular. The resultant displacement  $D_r$  of the specimen is obtained by resultant vector of normal displacement  $D_v$  and shear displacement  $D_h$ . The angle between resultant displacement  $D_r$  and crack affects the failure pattern. The angle increases firstly then decreases, and reaches a maximum when flaw angle is  $60^\circ$ . The larger the angle is, the more easily the tensile failure happens. On the contrary, the smaller the angle is, the more easily the shear failure happens. The failure normal stress

is also relevant to the angle and failure pattern as analyzed in Sect. 3.3.1.

### 3.1.3 Influence of Initial Stress

The influence of initial normal stress on failure pattern is revealed in group A, which is shown in Fig. 9. In low initial normal stress ( $\sigma_{ni} = 8, 16$  MPa), the exfoliation occurs around both the pre-existing flaw tips and the boundary of specimens (Fig. 9a, b). In medium initial normal stress ( $\sigma_{ni} = 24$  MPa), the exfoliation occurs only near the boundary of specimens (Fig. 9c). In high initial normal stress ( $\sigma_{ni} = 32, 40$  MPa), the exfoliation occurs around both the pre-existing flaw tips and the boundary of specimens except the tip of the pre-existing flaw near the loading side (Fig. 9d, f). The distributions of shear scratch correspond with that of exfoliation. There is a general variation trend from shear failure to tensile–shear mixed failure with the initial normal stress increasing.

The influence of initial shear stress on failure pattern is revealed in group B, which is shown in Fig. 10. There is an obvious increase of the area of exfoliation with the increase of the initial shear stress, and the position of exfoliation expands gradually from the boundary of the specimens to the pre-existing flaw tip. Correspondingly, the area of shear scratch also increases. The failure pattern generally changes from tensile failure to tensile–shear mixed failure, then to shear failure.

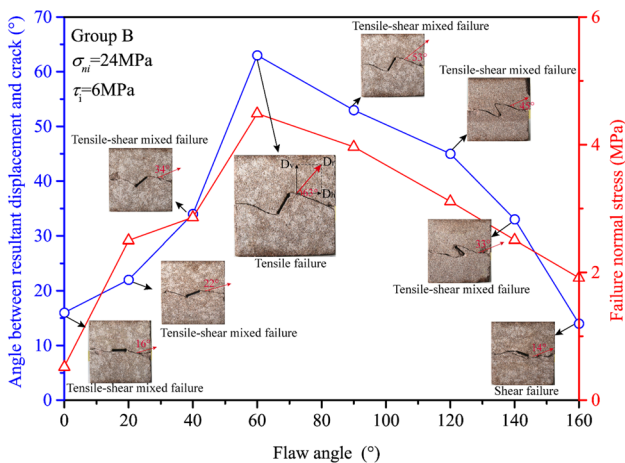


Fig. 8 Angle between resultant displacement and crack of specimens with different flaw angles

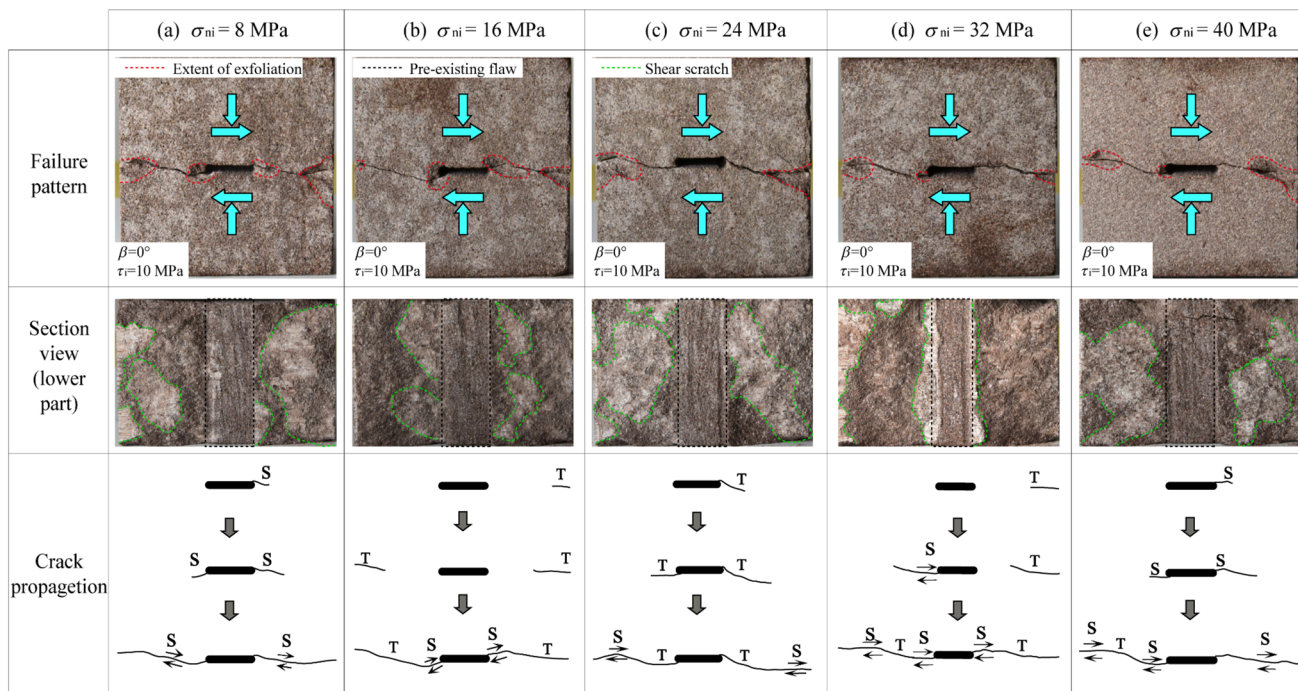
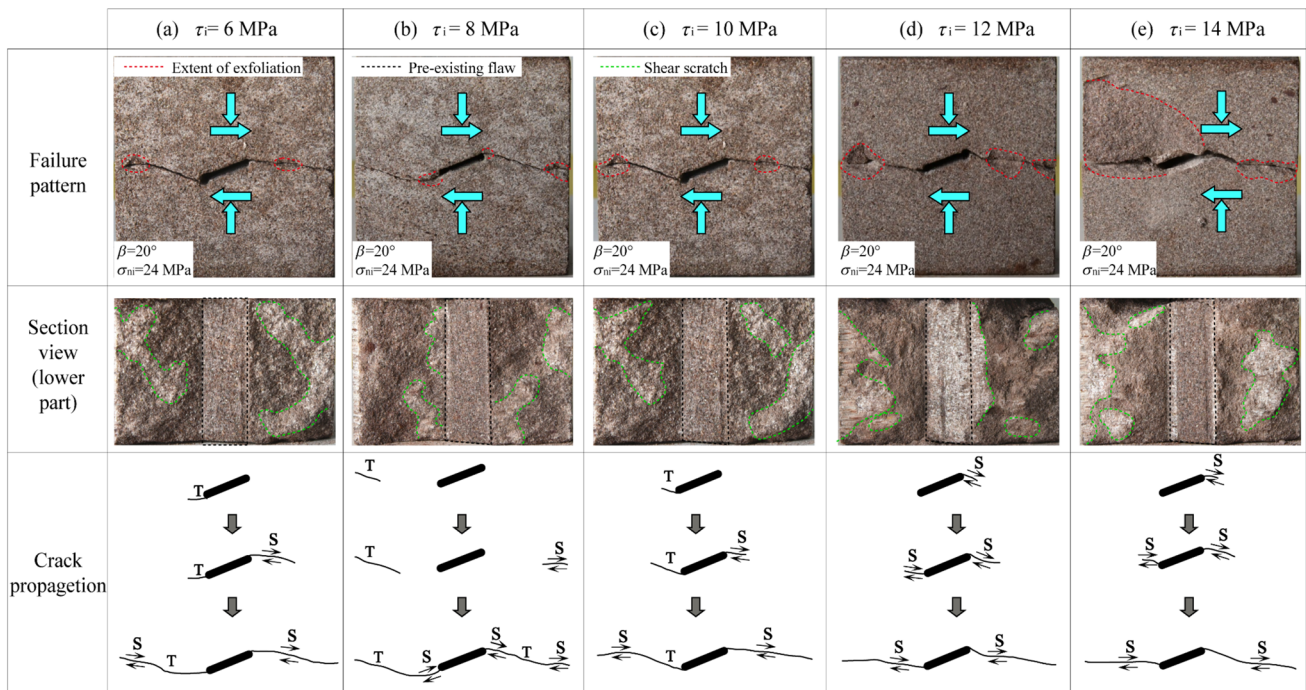
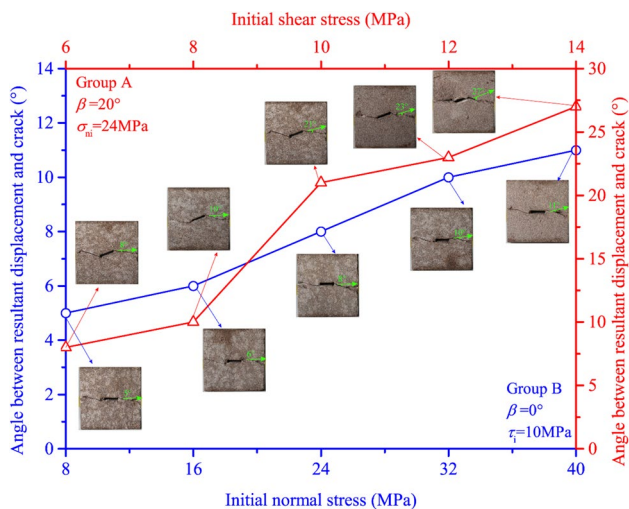


Fig. 9 Failure patterns of specimens with different initial normal stresses and same initial shear stress



**Fig. 10** Failure patterns of specimens with different initial shear stresses and same initial normal stress



**Fig. 11** Angle between resultant displacement and crack of specimens with different initial stress

The relationship between resultant displacement  $D_r$  and initial stress is shown in Fig. 11. The angle between resultant displacement  $D_r$  and crack increases with the increase of initial normal stress. In other words, the proportion of tensile failure will increase with the increase of initial normal stress. On the contrary, the angle decreases with initial shear stress. In other words, the proportion of shear failure will increase with the increase of initial shear stress.

## 3.2 Deformation

### 3.2.1 Evolution of Normal and Shear Displacements

Typical time history curves of normal and shear displacements are shown in Fig. 12. Three steps of the DSTUNS are divided by dotted line. As the time history curves of normal and shear displacement under different flaw angles and initial stress levels are similar, this section takes a working condition ( $\beta = 0^\circ$ ,  $\sigma_{ni} = 24$  MPa,  $\tau_i = 10$  MPa) as the example. Characteristics in each step are as follows:

- 1st step (section AB in Fig. 12). In the step of loading normal stress, the normal stress increases gradually to the target value, while the shear stress remains 0, thus the specimen is under uniaxial compression state. In the stage of compaction by initial loading, the deformation growth rate is relatively fast and the curve is convex. As the normal stress increases, the specimen gradually enters the stage of line elastic deformation. When the normal stress reaches the initial normal stress, the normal displacement reaches the maximum value.
- 2nd step (section BC (B'C') in Fig. 12). In the step of loading shear stress, the shear stress increases gradually to the target value, while the normal stress remains constant. With the increase of the shear stress, the normal displacement decreases slightly and linearly. The reason is that the shear plane climb along the surface of the



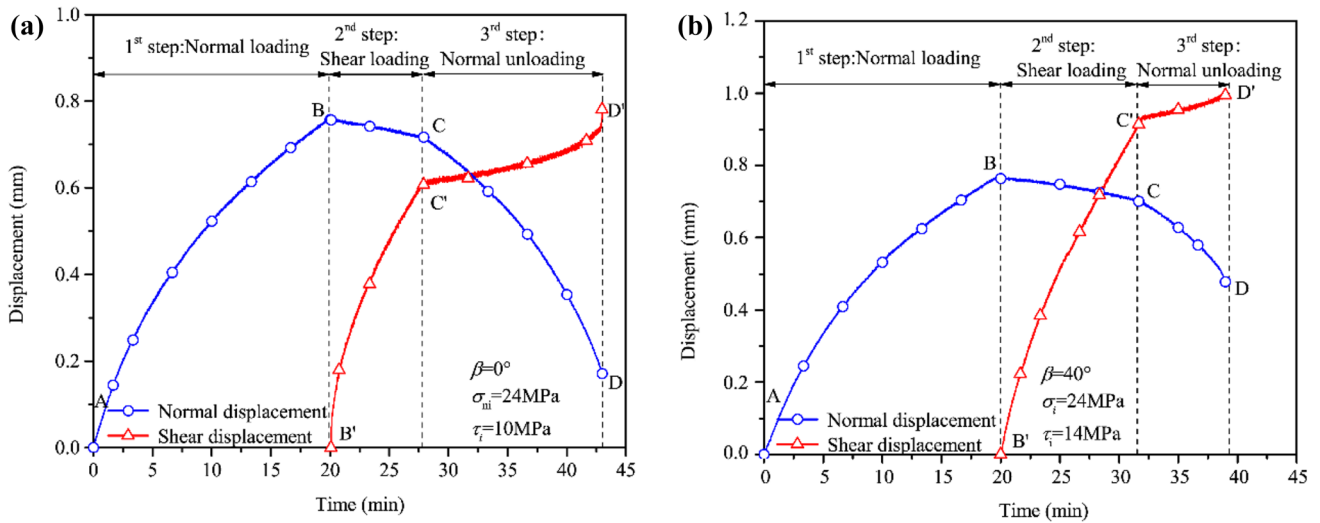


Fig. 12 Typical time history curves of normal and shear displacements

intergranular microdefects generating in the process of loading shear stress, resulting in the dilatancy and the decrease of the normal displacement.

- 3rd step (section CD (C'D') in Fig. 12). The step is the key one, in which the normal stress decreases until the specimen failing, while the shear stress remains constant. In this step, the normal displacement decreases obviously, while the shear displacement increases slowly. There are two main reasons for the obvious deformation in the direction of normal unloading: ① Elastic rebound deformation in the direction of normal unloading. ② The normal displacement caused by dilatancy. The decrease of normal stress causes the accumulation of shear displacement and the shear damage of the specimens, which result in the further decrease of normal displacement. The rates of normal and shear displacement during unloading were compared, it can be found that, before the occurrence of macroscopic fracture, the shear deformation rate is relatively slow,

while the normal unloading deformation rate is much faster. When the failure is imminent, the shear displacement increases rapidly, which indicates that unloading the normal stress reduces the resistance to shear failure of the specimen and leads to shear failure finally.

### 3.2.2 Peak Dilatancy Angle

Figure 13 shows the sketch of normal and shear displacements in each step of the DSTUNS. In this figure,  $\delta_{v1}$ ,  $\delta_{v2}$  and  $\delta_{v3}$  are the normal displacements, while  $\delta_{h1}$ ,  $\delta_{h2}$  and  $\delta_{h3}$  are the shear displacements in each step. Among these parameters,  $\delta_{v3}$  and  $\delta_{h3}$ , which are in the normal unloading step, should be focused on. Dilatancy behavior of dilatant material, such as rock and granular soils, appear to be associated with strength and deformation behaviors (Alejano and Alonso 2005). In addition, dilatancy plays an important role in the displacement variation of rock mass near the excavation boundary in the excavating engineering, such as tunnel

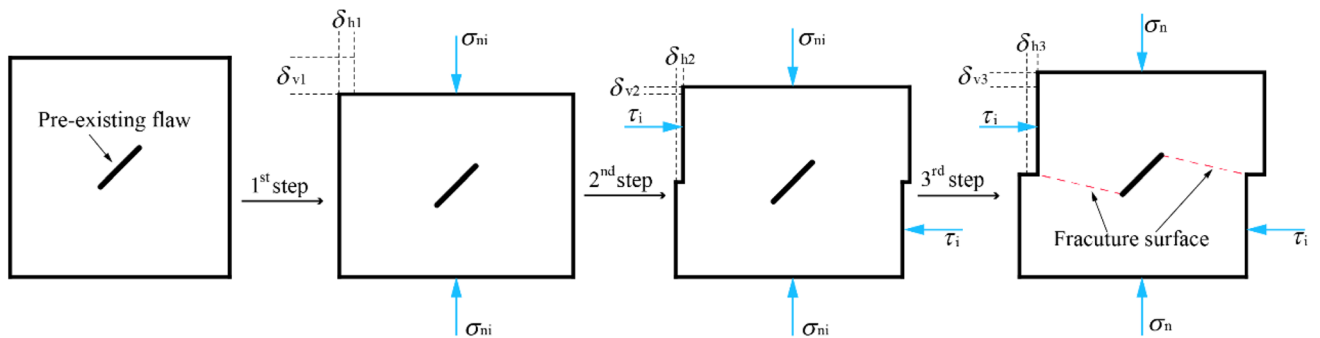


Fig. 13 Sketch of normal and shear displacements in the DSTUNS

excavation and deep mining (Alonso et al. 2003). Thus, the relationships between dilatancy angles and flaw angles, initial stress level will be studied in this section. Dilatancy angle can be defined as a parameter for describing a change in volume caused by the shear distortion of an element in rock material. The equation for calculating the dilatancy angle is as follows:

$$\psi = \arctan \frac{\delta_{v3}}{\delta_{h3}}, \tag{1}$$

where  $\psi$  is the dilatancy angle,  $\delta_{v3}$  and  $\delta_{h3}$  is the normal and shear displacement in the normal unloading step, respectively.

In the process of unloading, the volume expansion increases with the decrease of normal stress. In other words, the dilatancy angle increases and reaches the peak when the brittle failure of specimen happens. The relationships between the peak dilatancy angles  $\psi_{peak}$  and flaw angles, stress states are shown in Fig. 14a, b, respectively.

In the low initial normal stress level ( $\sigma_{ni} = 8$  MPa, 16 MPa), the peak dilatancy angle is sensitive to changes of the flaw angle, as shown in Fig. 14a. The peak dilatancy angle performs decreasing previously and increasing later with increasing the flaw angle. When  $\beta = 60^\circ$ , the peak dilatancy angle reaches minimum  $4.8^\circ$ . In other initial normal stress level ( $\sigma_{ni} = 24$  MPa, 32 MPa, 40 MPa), the peak dilatancy angle has the similar variation trend with the change of flaw angle, but the range is comparatively narrow.

The relationship between initial stress and peak dilatancy angle is shown in Fig. 14b. The peak dilatancy angle increases with the increase of initial normal stress. In the low initial normal stress ( $\sigma_{ni} = 8$  MPa, 16 MPa), increases in peak dilatancy angle is large with the increase of initial normal stress. In contrast, when the initial normal stress is larger than 24 MPa, the peak dilatancy angles remain stable with the increase of the initial normal stress. As for the initial shear stress, the peak dilatancy angles decrease with the increase of the initial shear stress. In the low initial shear stress ( $\tau_i = 6$  MPa, 8 MPa, 10 MPa), the peak dilatancy angles remain stable. In contrast, when the initial shear stress is larger than 10 MPa, the peak dilatancy angles have a big decrease.

### 3.3 Strength

#### 3.3.1 Failure Normal Stress

The failure normal stress  $\sigma_f$  is defined as the normal stress when the unloading failure happens. When the initial shear stress is same, the smaller the failure normal stress is, the more easily the specimen fails. It means that the shear strength is lower. Figure 15a, b shows the relationships

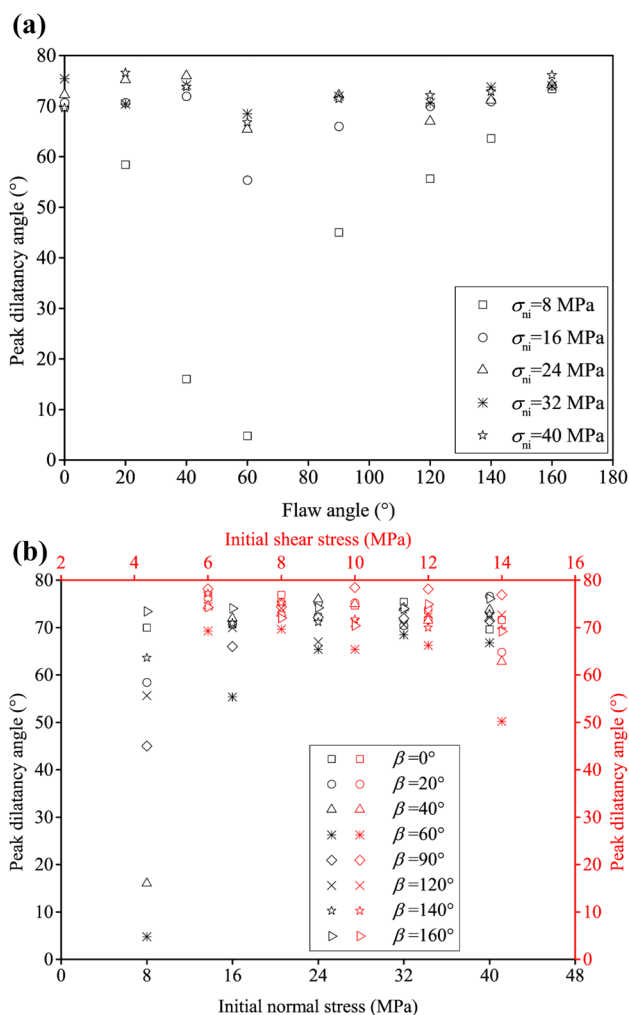


Fig. 14 Effects of flaw angle and initial stress on the peak dilatancy angle

between the failure normal stress  $\sigma_f$  and the flaw angle in group A and group B, respectively. There are the same variation trends in the two groups: increasing first and then decreasing. Among them, seven different flaw angles of specimens reach the maximum value at  $\beta = 60^\circ$ , and two different flaw angles of specimens reach the maximum value at  $\beta = 40^\circ$ . Contrast with the failure patterns in Sect. 3.3.1, when  $\beta = 40^\circ, 60^\circ$ , tensile–shear mixed failure and the tensile failure dominate. The results of strength in the DSTUNS match well with the results of failure patterns. The relationship between failure normal stress and flaw angle is also shown in Fig. 8. The variation trends of the angle between resultant displacement and crack, failure patten and failure normal stress maintain high consistency. The reason is that the tensile strength of rock is much less than the shear strength; therefore, the specimen with tensile failure patten has a high failure normal stress (namely a low unloading

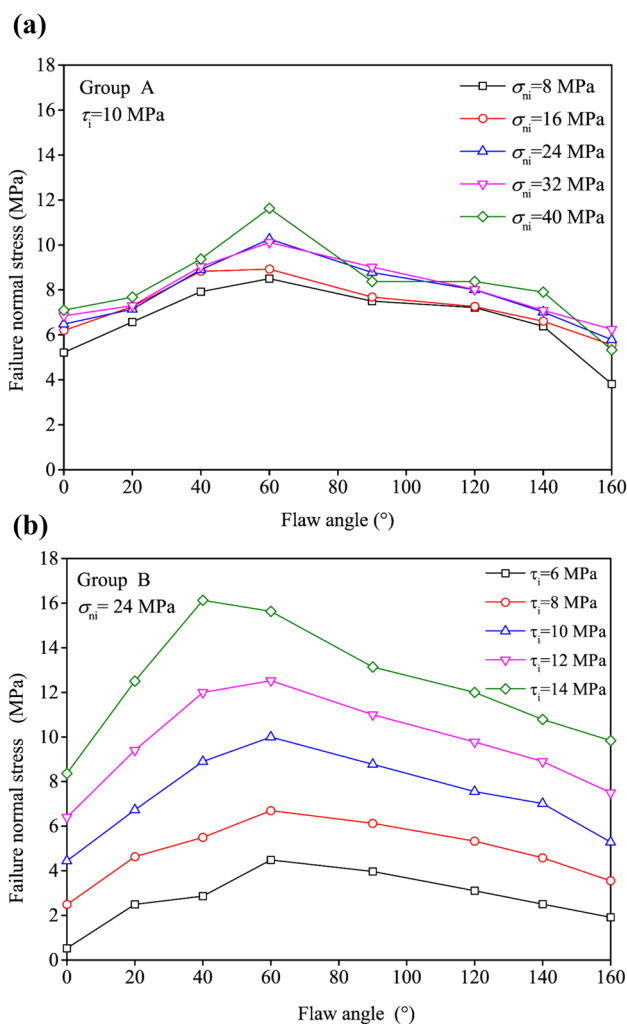


Fig. 15 Effect of flaw angle on the failure normal stress in two groups

quantity of normal stress) and a large angle between resultant displacement and crack.

### 3.3.2 Shear Strength Parameters

Figure 16a, b shows the relationships between the failure normal stress and the initial stress in group A and group B, respectively. In group A, there are the same initial shear stress and five different initial normal stresses. The failure normal stress increases with the increase of the initial normal stress, it is related to the internal damage of rock in the normal loading step. In group B, there are the same initial normal stress and five different initial shear stresses, the failure normal stress increases linearly with the increase of the initial shear stress. On the basis of Mohr–Coulomb failure criterion, shear strength parameters are obtained by linear fitting, as shown in Fig. 17.

The relationship between the shear strength parameters and the flaw angles is shown in Fig. 17. Internal friction

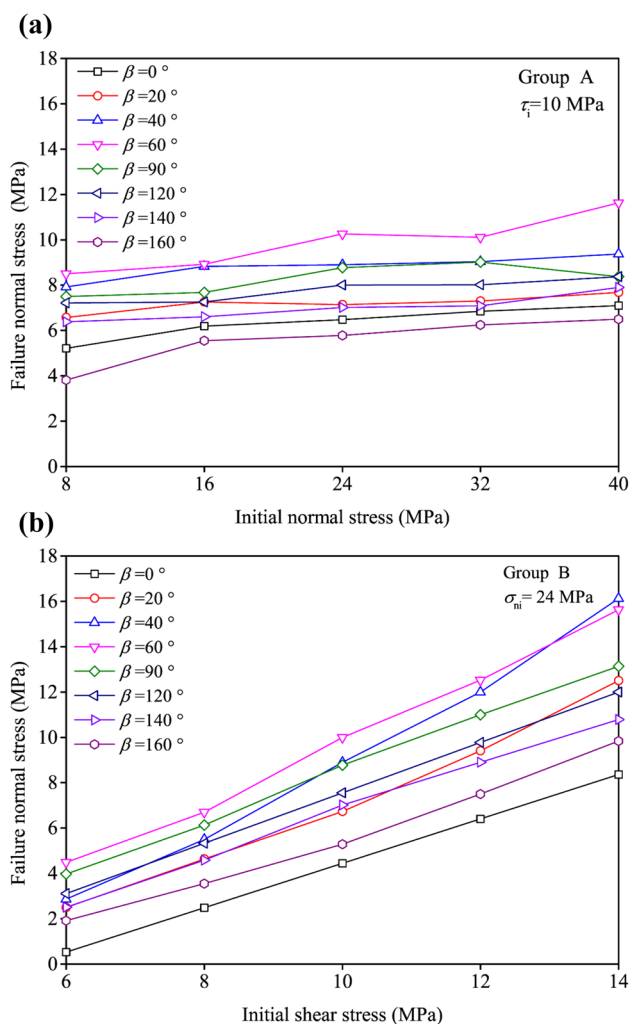


Fig. 16 Effect of initial stress level on the failure normal stress in two groups

angle and cohesion both decrease firstly and then increase as the flaw angle goes up. The minimum values of internal friction angle and cohesion are reached when  $\beta = 40^\circ$  and  $\beta = 90^\circ$ , respectively. The fitting equation can be expressed as follows:

$$\begin{cases} c(\beta) = 2 \times 10^{-6} \beta^3 - 0.0002 \beta^2 - 0.0215 \beta + 5.5468 \\ \varphi(\beta) = 4 \times 10^{-7} \beta^4 - 0.0002 \beta^3 + 0.0219 \beta^2 - 1.0034 \beta + 45.393. \end{cases} \quad (2)$$

In addition, the M–C criterion can be expressed as follows:

$$\tau_f(\beta) = \tan[\varphi(\beta)]\sigma_f + c(\beta). \quad (3)$$

As the failure normal stress plays an important role in measuring the shear strength in the DSTUNS, when the initial shear stress (ISS) is same, then transform the Eq. 3–4 as follows:

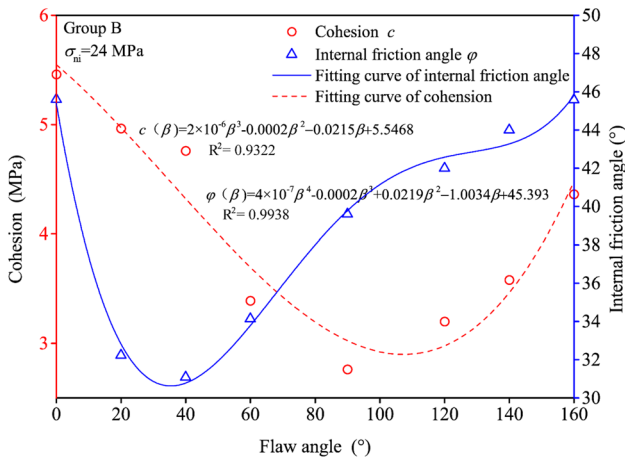


Fig. 17 Fitting curves of shear strength parameters

$$\sigma_f = \frac{\tau_f - c(\beta)}{\tan \varphi(\beta)} \quad (4)$$

Substituting Eq. 2 into Eq. 4, using Python as the programming language to solve the extreme value of Eq. 4. The result is that the maximum value is obtained when  $\beta = 55.9^\circ$ , which is accordance with the result of Fig. 15.

## 4 Discussion

### 4.1 Differences of Failure Between DSTUNS and DSTCNS

The stress path of the DSTUNS and the DSTCNS is different, which may result in the differences of the mechanical behaviors of rock specimens in these two tests. Failure pattern from the DSTUNS and the DSTCNS under the same normal stress condition (24 MPa), as well as the corresponding lower part section view and sketch of cracks are summarized in Fig. 18. The differences of failure between the DSTUNS and the DSTCNS mainly perform in following aspects:

1. *Branch crack* In the DSTUNS, branch cracks appear only when  $\beta = 0^\circ, 160^\circ$  (Fig. 18a, h), they initiate from the loading side and extend to the middle of the upper part of specimens. In contrast, in the DSTCNS, branch cracks appear nearly all flaw angles conditions (except  $\beta = 20^\circ, 120^\circ, 160^\circ$ ). The initiations and extensions are diversified: initiating from the flaw tip (Fig. 18a, d); initiating from the loading side (Fig. 18e, g); initiating far from the loading side (Fig. 18c, e).
2. *Extent of exfoliation* Exfoliation in the DSTCNS is more serious than that in the DSTUNS. Most extents of exfoliation in the DSTUNS distribute on the two sides of specimens, while exfoliation in the DSTCNS also

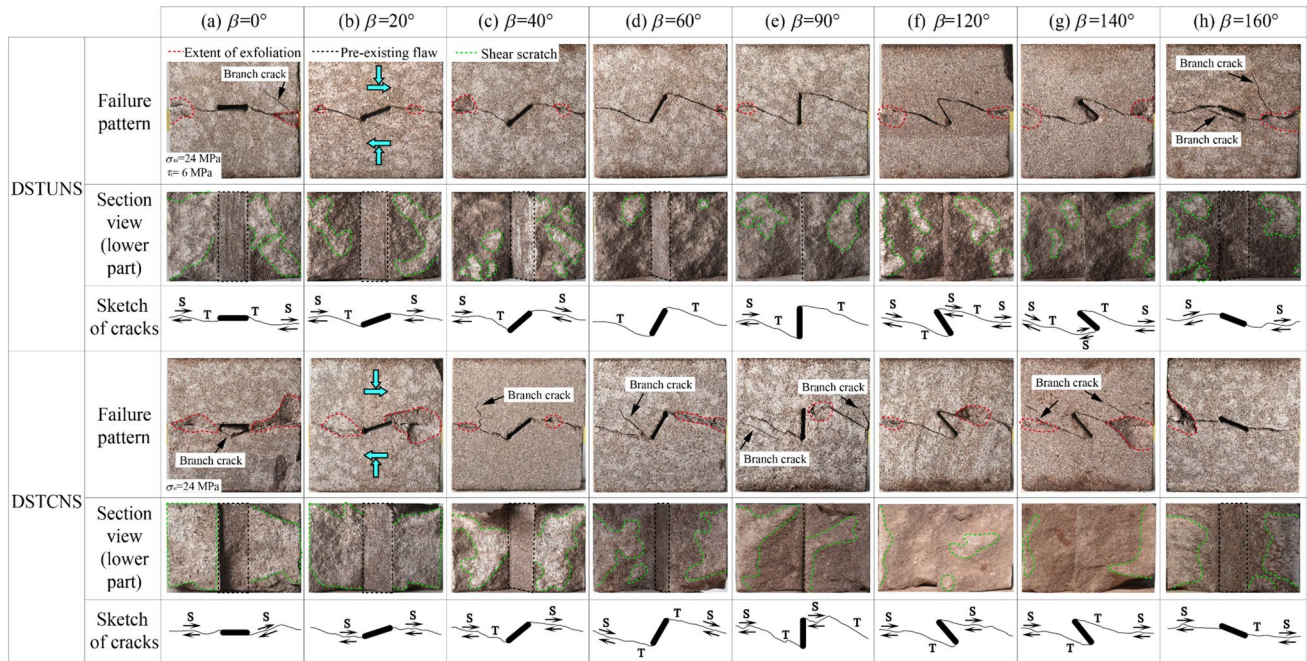


Fig. 18 Comparison of failure patterns between the DSTUNS and the DSTCNS

appears near the flaw tip (Fig. 18e) and the middle of the crack (Fig. 18c, f).

3. *Shear scratch* The proportion of shear scratch in the DSTCNS is more than that in the DSTUNS. In addition, the distributing of shear scratch in the DSTUNS is dispersal and asymmetrical. On the contrary, the distributing of shear scratch in the DSTCNS is centralized and symmetrical.
4. *Failure pattern* The influence of stress path on crack segments is revealed, which are shown in Fig. 18. In the DSTUNS, there are three main failure patterns: shear failure pattern (Fig. 18h); tensile failure pattern (Fig. 18d); tensile–shear mixed failure pattern (Fig. 18a, b, c, e, f, and g). In the DSTCNS, there are only two failure patterns: shear failure pattern (Fig. 16a, b); tensile–shear mixed failure pattern (Fig. 18c–g and h).
5. When the flaw angle is same, the proportion of tensile crack in the DSTUNS is larger than that in the DSTCNS. Relatively, the proportion of shear crack in the DSTUNS is smaller than that in the DSTCNS. In other words, tensile failure dominates in the DSTUNS, while shear failure dominates in the DSTCNS.

### 4.2 Differences of strength between DSTUNS and DSTCNS

Figure 19 shows the fitting failure envelopes in the DSTCNS and the DSTUNS (group B and  $\beta = 90^\circ$ ). In the same flaw angle condition, the internal friction angle in group B of the DSTUNS is 14.2% less than that in the DSTCNS; however, the cohesion in group B of the DSTUNS is 52.6% higher than that in the DSTCNS. It is revealed that the stress path has effects on the shear strength parameters. Additionally, strength weakening takes place in the process of DSTUNS compared with DSTCNS. As Fig. 19 shows that failure shear stress  $\tau_f$  in the DSTUNS is smaller than that in the DSTCNS when the failure normal stress  $\sigma_f$  is same. One reason is that there is higher initial normal stress in the DSTUNS than that in the DSTCNS, it would cause the internal damage (mainly micro cracks) which reduces the strength of specimens. The other reason is that unloading leads to rebound and dilatancy along the normal direction, the tensile stress caused in that process will reduce the strength of specimens.

The strength weakening effect under DSTUNS suggests that the shear strength parameters used in stability evaluation of rock excavation engineering should be determined by unloading tests. The DSTCNS may lead to an excessive shear strength compared with the actual strength. Two fitting curves of DSTUNS and DSTCNS are not parallel, as shown in Fig. 19. The reduction degree of shear strength decreases with the increase of normal stress. The reason is that larger normal stress causes compaction effect which enhances the resistance to shear failure.

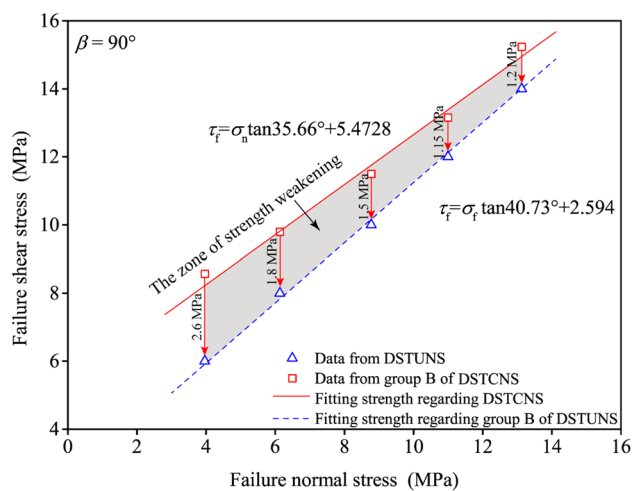


Fig. 19 Fitting failure envelopes in the DSTCNS and the DSTUNS

### 5 Conclusions

This paper focuses on the mechanical behaviors of sandstone specimens containing single pre-existing flaw under unloading normal stress with constant shear stress. The effects of flaw angle and initial normal and shear stresses were investigated. High speed camera was used to capture the details of cracking process. The key conclusions are summarized as follows:

1. Five failure patterns can be summarized in response to different flaw angles and initial stress levels. The variation trends change from shear failure to tensile–shear mixed failure, then to tensile failure, finally change to shear failure again with the increase of the flaw angle. The angle between resultant displacement and crack plays a leading role in the variation trends.
2. The peak dilatancy angle performs decreasing previously and increasing later with increasing the flaw angle. The peak dilatancy angle increases and decreases with the increase of the initial normal and shear stresses, respectively.
3. When the flaw angle is  $60^\circ$ , the shear strength is the lowest. Internal friction angle and cohesion both decrease firstly and then increase with the increase of the flaw angle. The minimum values are reached when  $\beta = 40^\circ$  and  $\beta = 90^\circ$ , respectively.
4. The differences of failure between the DSTUNS and the DSTCNS mainly perform in branch crack, extent of exfoliation, shear scratch and failure pattern. Shear strength weakening takes place in DSTUNS compared with DSTCNS.

**Acknowledgements** The present work is supported by the National Natural Science Foundation of China (Nos. 41972297, 41807279 and 41672300), the Supporting program of hundred promising innovative talents in Hebei provincial education office (No. SLRC2019027) and the Natural Science Foundation of Hebei Province (No. E2019202336).

## References

- Alejano LR, Alonso E (2005) Considerations of the dilatancy angle in rocks and rock masses. *Int J Rock Mech Min Sci* 42(4):481–507
- Alonso E, Alejano LR, Varas F, Fdez-Manin G, Carranza-Torres C (2003) Ground response curves for rock masses exhibiting strain-softening behaviour. *International Journal for Numerical and Analytical Methods in Geomechanics* 27(13):1153–1185
- Cai M, Kaiser PK (2005) Assessment of excavation damaged zone using a micromechanics model. *Tunnel Undergr Sp Technol Incorp Trench Technol Res* 20(4):301–310
- Cen DF, Huang D, Song YX, Jiang QH (2020) Direct tensile behavior of limestone and sandstone with bedding planes at different strain rates. *Rock Mech Rock Eng*. <https://doi.org/10.1007/s00603-020-02070-x>
- Cen DF, Huang D (2017) Direct shear tests of sandstone under constant normal tensile stress condition using a simple auxiliary device. *Rock Mech Rock Eng* 50(6):1425–1438
- Cho N, Martin CD, Sego DC (2008) Development of a shear zone in brittle rock subjected to direct shear. *Int J Rock Mech Min Sci* 45(8):1335–1346
- Gehle C, Kutter HK (2003) Breakage and shear behavior of intermittent rock joints. *Int J Rock Mech Min Sci* 40(5):687–700
- Huang RQ, Huang D (2014) Evolution of Rock Cracks Under Unloading Condition. *Rock Mech Rock Eng* 47(2):453–466
- Huang D, Li Y (2014) Conversion of strain energy in triaxial unloading tests on marble. *Int J Rock Mech Min Sci* 66:160–168
- Huang D, Zhu TT (2018) Experimental and numerical study on the strength and hybrid fracture of sandstone under tension-shear stress. *Eng Fract Mech* 200:387–400
- Huang D, Zhu TT (2019) Experimental study on the shear mechanical behavior of sandstone under normal tensile stress using a new double-shear testing device. *Rock Mech Rock Eng* 52(9):3467–3474
- Huang D, Li YQ, Song YX, Xu Q, Pei XJ (2019) Insights into the catastrophic Xinmo rock avalanche in Maoxian county, China: combined effects of historical earthquakes and landslide amplification. *Eng Geol* 258:105158
- Huang D, Cen DF, Song YX (2020) Comparative investigation on the compression–shear and tension–shear behaviour of sandstone at different shearing rates. *Rock Mech Rock Eng*. <https://doi.org/10.1007/s00603-020-02094-3>
- Park KH, Tontavanich B, Lee JG (2008) A simple procedure for ground response curve of circular tunnel in elastic-strain softening rock masses. *Tunn Undergr Space Technol* 23(2):151–159
- Wong RHC, Chau KT (1998) Crack coalescence in a rock—like material containing two cracks. *Int J Rock Mech Min Sci* 35(2):147–164
- Wong RHC, Chau KT, Tang CA, Lin P (2001) Analysis of crack coalescence in rock-like materials containing three flaws—part I: experimental approach. *Int J Rock Mech Min Sci* 38(7):909–924
- Wong LNY, Einstein HH (2009) Crack coalescence in molded gypsum and carrara marble: part I. Macroscopic observations and interpretation. *Rock Mech Rock Eng* 42(3):475–511
- Wong RHC, Huang ML, Jiao MR, Tang CA, Zhu WS (2004a) The mechanisms of crack propagation from surface 3D fracture under uniaxial compression. *Key Eng Mater* 261–263:219–224
- Wong RHC, Law CM, Chau KT, Zhu WS (2004b) Crack propagation from 3D surface fractures in PMMA and marble specimens under uniaxial compression. *Int J Rock Mech Min Sci* 41(3):360–366
- Yin Q, Ma G, Jing H, Wang H, Su H, Wang Y, Liu R (2017) Hydraulic properties of 3D rough-walled fractures during shearing: an experimental study. *J Hydrol* 555:169–184
- Yin Q, Jing H, Ma G, Su H, Liu R (2018) Investigating the roles of included angle and loading condition on the critical hydraulic gradient of real rock fracture networks. *Rock Mech and Rock Eng* 51(10):3167–3177
- Yin Q, Liu R, Jing H, Su H, Yu L, He L (2019) Experimental study of nonlinear flow behaviors through fractured rock samples after high temperature exposure. *Rock Mech and Rock Eng* 52: 2963–2983
- Zeng B, Huang D, Ye SQ, Chen FY, Zhu TT, Tu YL (2019) Triaxial extension tests on sandstone using a simple auxiliary apparatus. *Int J Rock Mech Min Sci* 120:29–40
- Zhou XP, Cheng H, Feng YF (2014) An Experimental study of crack coalescence behavior in rock-like materials containing multiple cracks under uniaxial compression. *Rock Mech Rock Eng* 47(6):1961–1986
- Zhu T, Huang D (2019) Experimental investigation of the shear mechanical behavior of sandstone under unloading normal stress. *Int J Rock Mech Min Sci* 114:186–194
- Zhong Z, Huang D, Zhang Y, Ma G (2020) Experimental study on the effects of unloading normal stress on shear mechanical behaviour of sandstone containing a parallel fissure pair. *Rock Mech and Rock Eng* 53:1647–1663

**Publisher's Note** Springer Nature remains neutral with regard to jurisdictional claims in published maps and institutional affiliations.